PNAS RESEARCH ARTICLE | MEDICAL SCIENCES OPEN ACCESS

Biochemical analysis of EGFR exon20 insertion variants insASV and insSVD and their inhibitor sensitivity

Hanchen Zhao[a,b], Tyler S. Beyett[a,b,1], Jie Jiang[c,d,e], Jaimin K. Rana[a], Ilse K. Schaeffner[a], Jhasmer Santana[a], Pasi A. Jänne[c,d,e], and Michael J. Eck[a,b,2]

Affiliations are included on p. 10.

Edited by Joseph Schlessinger, Yale School of Medicine, New Haven, CT; received August 24, 2024; accepted September 30, 2024

Somatic mutations in the epidermal growth factor receptor (EGFR) are a major cause of non–small cell lung cancer. Among these structurally diverse alterations, exon 20 insertions represent a unique subset that rarely respond to EGFR tyrosine kinase inhibitors (TKIs). Therefore, there is a significant need to develop inhibitors that are active against this class of activating mutations. Here, we conducted biochemical analysis of the two most frequent exon 20 insertion variants, V769_D770insASV (insASV) and D770_N771insSVD (insSVD) to better understand their drug sensitivity and resistance. From kinetic studies, we found that EGFR insASV and insSVD are similarly active, but have lower $K_{m,\ ATP}$ values compared to the L858R variant, which contributes to their lack of sensitivity to 1st-3rd generation EGFR TKIs. Biochemical, structural, and cellular studies of a diverse panel of EGFR inhibitors revealed that the more recently developed compounds BAY-568, TAS6417, and TAK-788 inhibit EGFR insASV and insSVD in a mutant-selective manner, with BAY-568 being the most potent and selective versus wild-type (WT) EGFR. Cocrystal structures with WT EGFR reveal the binding modes of each of these inhibitors and of poziotinib, a potent but not mutantselective inhibitor, and together they define interactions shared by the mutant-selective agents. Collectively, our results show that these exon20 insertion variants are not inherently inhibitor resistant, rather they differ in their drug sensitivity from WT EGFR. However, they are similar to each other, indicating that a single inhibitor should be effective for several of the diverse exon 20 insertion variants.

lung cancer | EGFR inhibitors | enzymology | X-ray crystallography

Significance

Mutant-selectivity is a key requirement for a successful inhibitor targeting oncogenic epidermal growth factor receptor (EGFR) variants in lung cancer, because inhibition of wild-type EGFR systemically is the dose-limiting toxicity of most EGFR tyrosine kinase inhibitors (TKIs). We find that a small subset of EGFR TKIs including BAY-568, TAS6417, and TAK-788 inhibit the insASV, insSVD, and insNPG variants in a mutant-selective manner. By contrast, poziotinib and BDTX-189 are equally or more potent inhibitors of wild-type EGFR, which, consistent with clinical experience, predicts a narrow or nonexistent therapeutic window for these agents. Overall, our findings suggest that searching de novo for novel exon 20 insertion inhibitor scaffolds may be a more productive route to mutant-selectivity than evolution of existing EGFR inhibitors.

Cancer is one of the leading causes of death across the world, and among various types of cancer, lung cancer contributes most to the overall cancer-related deaths, with approximately 2.2 million new cases diagnosed and 1.8 million deaths each year worldwide (1). Non–small cell lung cancer (NSCLC) is the most common type of lung cancer and accounts for about 85% of all lung cancer cases (2). Somatic mutations in the epidermal growth factor receptor (EGFR) are a frequent driver of NSCLC and are present in ~12 to 50% of NSCLC, with the higher prevalence of EGFR mutation in Asian populations (3–6). These mutations cause constitutive activation of EGFR, thus promoting downstream signaling to Erk and enhancing antiapoptotic signals, which contribute to oncogenesis. The L858R point mutation and deletions in exon 19 are the two most common oncogenic EGFR alterations, which collectively represent approximately 85% of all EGFR mutations globally (6). As the third-most common mutation type, exon 20 insertions represent 6 to 12% of all EGFR mutants and account for around 10,000 new cases of NSCLC annually worldwide (7–9).

In general, tumors driven by the L858R mutation or exon 19 deletions in EGFR show clinical response to treatment with 1st and 2nd generation of EGFR tyrosine kinase inhibitors (TKIs) gefitinib, erlotinib, and afatinib (3, 4, 10–12). These alterations in the kinase domain of EGFR decrease its affinity for adenosine triphosphate ATP measured by an increased $K_{m,\ ATP}$ value as compared to wild-type (WT) EGFR and thereby sensitize to treatment with ATP-competitive TKIs (13–15). Because inhibition of WT EGFR is the dose-limiting toxicity for these agents, this sensitization relative to WT EGFR affords a crucial therapeutic window (16). The treatment-acquired T790M mutation closes this therapeutic window, in part by restoring ATP affinity and in part by decreasing affinity for 1st and 2nd generation EGFR TKIs (17). Third-generation EGFR TKIs were developed to address the T790M mutation via their intrinsic selectivity for mutant EGFR over wild type and their irreversible mechanism of action (18, 19). Third-generation agent osimertinib was initially approved in this resistance setting (20), and has now become 1st-line therapy for patients whose tumors harbor EGFR L858R or exon19 deletion (21, 22). More recently, allosteric inhibitors (23, 24) and 4th generation EGFR TKIs (25) have

This article is a PNAS Direct Submission.

[1]Present address: Department of Pharmacology and Chemical Biology, Emory University School of Medicine, Atlanta, GA 30322.

[2]To whom correspondence may be addressed. Email: michael_eck@dfci.harvard.edu.

This article contains supporting information online at https://www.pnas.org/lookup/suppl/doi:10.1073/pnas.2417144121/-/DCSupplemental.

Published October 29, 2024.

emerged as a strategy to overcome the C797S mutation that can confer resistance to Osimertinib (26, 27). Unfortunately, most tumors harboring insertions in exon 20 show limited clinical response to these TKIs (7, 9, 28), which were developed primarily for the sensitizing exon19 deletion and/or L858R variants. Thus, there remains a clinical need for small-molecule kinase inhibitors that potently and selectively target exon 20 insertion variants (29–31). Additionally, unlike L858R and exon 19 deletions, exon 20 insertion variants have not been extensively studied biochemically, and our understanding of their kinetic properties and drug sensitivity is incomplete.

EGFR exon 20 insertions are structurally heterogeneous and include insertions of 1 to 7 residues in the region from D761 to C775 (32). Although many rare insertions of have been identified, the two most common account for about 40% of all exon 20 variants (7). These are the V769_D770insASV (insASV) and D770_N771insSVD (insSVD) insertions, which introduce three additional residues (e.g., Ala-Ser-Val or Ser-Val-Asp) in the indicated locations. This insertion site lies in the αC-β4 loop just after the C-helix of the kinase domain. Clinical data indicate that both are resistant to the 1st–3rd generation TKIs (33–35). We previously determined the crystal structure of EGFR D770_N771insNPG (insNPG), a rare exon 20 insertion mutant that occurs in the same site as insSVD and shares similar TKI resistance with the insASV and insSVD mutants in vitro (28). The structure revealed that the inserted residues form a wedge at the end of the C-helix that appears to promote its inward, active orientation, but provided little insight into its lack of sensitivity to existing EGFR TKIs, as the insertion leaves the ATP binding pocket unaltered.

Over the past few years, several inhibitors targeting exon 20 insertions have entered preclinical or clinical studies, including BDTX-189 (36), poziotinib (30), TAS6417 (CLN-081, zipalertinib) (31), BAY 2476568 (BAY-568) (37), BAY2927088 (38), DZD9008 (sunvozertinib) (39, 40), and TAK-788 (mobocertinib) (29). TAK-788 had received accelerated FDA approval for certain patients with exon 20 insertions (41), but it was subsequently withdrawn from the market after a phase III trial failed to meet its primary endpoint (42). Recently, the FDA granted breakthrough therapy designation to sunvozertinib as a frontline treatment for advanced or metastatic NSCLC driven by exon 20 insertion mutations (40). BAY2927088 is being studied in NSCLC patients with EGFR and Her2 exon20 insertions, but its chemical structure has not been disclosed.

The activity of EGFR TKIs has been extensively assessed in exon 20 insertion variants in a cellular context (30, 43), but relatively little information is available regarding the biochemical properties and TKI-sensitivity of the purified EGFR kinase domain bearing common exon 20 insertions. To better understand the effects of the insASV and insSVD insertions on the activity and drug sensitivity of the mutant kinase, we kinetically characterized the EGFR insASV and insSVD kinases and assessed their sensitivity to a broad panel of EGFR TKIs in biochemical assays. We find that insASV and insSVD are 38- and 27-fold more active than the WT EGFR kinase, respectively, with $K_{m,\,ATP}$ values intermediate between those of the WT kinase and the inhibitor-sensitized L858R mutant. Biochemical, structural, and cellular studies of a diverse panel of EGFR inhibitors revealed that BAY-568, BAY-33, TAS6417, and TAK-788 inhibit EGFR insASV and insSVD in a mutant-selective manner, with BAY-568 being the most potent and mutant selective. Cocrystal structures of BAY-33, TAK-788, TAS6417, and poziotinib with WT EGFR reveal the binding poses and key interactions of these inhibitors, but do not yield a clear structural understanding of their mutant-selectivity or lack thereof. Collectively, our results provide a side-by-side comparison of the potency and mutant-selectivity of several agents developed as exon 20 inhibitors and show that insASV and insSVD are not inherently drug-resistant. Rather, they differ in their inhibitor sensitivity as compared with the "classical" exon 19 deletion and L858R point variants and WT EGFR, which are more similar to one another.

Results

Enzyme Preparation and Kinetic Analysis of EGFR insASV and insSVD. Difficulty in obtaining the mutant kinase domains in soluble, active form has been an obstacle in biochemical characterization of EGFR insASV and insSVD. To overcome this challenge, we prepared constructs for baculoviral/insect cell expression spanning different residue ranges and with differing affinity purification tags, and we also explored a range of insect cell infection conditions and buffer compositions. Ultimately, we succeeded with a construct spanning EGFR residues 696 to 1,022, which has been widely used for preparation of WT EGFR and other mutants, but with inclusion of 20% glycerol in the purification buffer. This higher concentration of glycerol was required to prevented aggregation of EGFR insASV and insSVD proteins (*Materials and Methods* and *SI Appendix*, Fig. S1).

We used a coupled enzyme assay to determine enzyme kinetic parameters for these exon 20 insertions, as well as for WT, L858R, and L858R/T790M EGFR for comparison. This well-established continuous assay employs pyruvate kinase and lactate dehydrogenase to couple ADP production to oxidation of NADH to NAD+, which is measured as a decrease in absorbance at 340 nM (44). We used poly(Glu_4,Tyr_1) as a peptide substrate at a concentration of 5 mM. Reaction velocities at increasing ATP concentrations were plotted to determine Michaelis–Menten kinetic parameters (Table 1 and *SI Appendix*, Fig. S2 *A–F*). Both insASV and insSVD were highly active as compared with WT EGFR (with catalytic rates K_{cat} that are 38- and 27-fold higher that WT, respectively), and were comparable to the L858R variant (41-fold higher that WT). $K_{m,\,ATP}$ values for the insertion variants were increased relative to WT EGFR, but their catalytic efficiencies ($k_{cat}/K_{m,\,ATP}$) were nevertheless sixfold higher due to their much faster catalytic rates (Table 1).

Table 1. Enzyme kinetic parameters of WT and mutant EGFR kinases*

	k_{cat} (s^{-1})	Fold activity versus WT	$K_{m,\,ATP}$ (μM)	$k_{cat}/K_{m,\,ATP}$ (s^{-1} μM^{-1})	$K_{m,\,peptide}$ (μM)
WT	0.026 ± 0.002	1	6 ± 4	0.004 ± 0.0003	>5,000
insASV	0.994 ± 0.079	38	39 ± 12	0.026 ± 0.002	489 ± 148
insSVD	0.710 ± 0.041	27	27 ± 7	0.026 ± 0.002	212 ± 43
L858R	1.063 ± 0.057	41	79 ± 14	0.014 ± 0.0007	3,542 ± 1,129
L858R/T790M	0.880 ± 0.093	34	15 ± 7	0.059 ± 0.0062	481 ± 238

*Values shown are mean ± SD, n = 3.

The enhanced inhibitor sensitivity of EGFR L858R and exon 19 deletions stems, at least in part, from their decreased affinity for ATP compared to the WT EGFR (13, 14). While the $K_{m,\ ATP}$ values of insASV and insSVD are higher as compared with WT EGFR, they are lower than that of the highly sensitive L858R mutant (Table 1). This indicates a relatively higher affinity for ATP than L858R EGFR, and likely contributes to their diminished sensitivity to EGFR TKIs as compared with the L858R and exon 19 deletion variants. We observed similar results in our prior biochemical evaluation of the insNPG variant (28). Interestingly, both insASV and insSVD exhibited markedly lower $K_{m,peptide}$ values than WT or L858R EGFR. Together with their enhanced catalytic rates, this may contribute to their oncogenicity.

Biochemical Sensitivity of EGFR insASV, insSVD, and insNPG to EGFR Inhibitors. We measured the biochemical potencies of a diverse panel of EGFR inhibitors against insASV, insSVD, and insNPG exon 20 insertion mutants and for comparison against WT EGFR and the L858R and L858R/T790M point mutants. Inhibitors selected for evaluation include representative 1st-4th generation compounds, allosteric inhibitors, and six compounds developed as exon 20 insertion inhibitors (*SI Appendix*, Figs. S3 and S4). We used the recombinant EGFR kinase proteins as described above in a homogeneous time-resolved fluorescence (HTRF) assay to obtain dose–response curves for these inhibitors. These assays were carried out with 1 mM ATP to approximate cellular concentrations of this substrate. The resulting IC_{50} values are presented in Table 2, and the underlying dose–response curves for the six exon 20 insertion inhibitors are presented in Fig. 1. Complete dose–response data are provided in *SI Appendix*, Fig. S3.

As might be expected, the exon 20 inhibitors were overall most potent against the exon 20 insertion variants, with IC_{50} values typically in the single-digit nanomolar range (Fig. 1 and Table 2). Exceptions to this were TAS6417, which inhibited the insASV mutant with an IC_{50} of 16 nM (as compared to 6 nM for insSVD), and BDTX-189, which inhibited the insSVD mutant with an IC_{50} of 55 nM (as compared to 2.1 nM for insASV). Interestingly, the recently disclosed compound BAY-568 (37) exhibited subnanomolar potency against all three insertion variants, with a wide margin of selectivity versus WT EGFR (IC_{50} > 1 μM). BAY-33, a close analog of BAY-568 that we synthesized based on a patent application prior to disclosure of BAY-568 (45), exhibited a similar pattern of selectivity, albeit with 4- to 10-fold reduced potency as compared with BAY-568 (Fig. 1 *A* and *B* and Table 2). TAS6417 and TAK-788 exhibited a more modest degree of selectivity versus WT EGFR, in the range of twofold to eightfold for TAS6417 and approximately threefold for TAK-788 (Fig. 1 *C* and *D* and Table 2). By contrast, poziotinib and BDTX-189 showed no selectivity; they were equipotent or more potent against WT EGFR than against the insertion variants (Fig. 1 *E* and *F* and Table 2). This is not entirely unexpected, as both are irreversible inhibitors that share the anilinoquinazoline core found in many 2nd generation EGFR TKIs that are also potent inhibitors of WT EGFR (Table 2 and *SI Appendix*, Fig. S4). Among 1st-3rd generation EGFR TKIs, a few were potent against one or more of the exon 20 insertion variants, including lapatinib, neratinib, and mavelertinib. Additionally, allosteric inhibitor JBJ-09-063 inhibited insASV with an IC_{50} of 28 nM. However, none of these agents were selective versus WT EGFR.

To better understand the degree of correlation in drug sensitivity across WT and various EGFR mutants, we plotted pairwise comparisons of IC_{50} values (Fig. 2). This analysis revealed little if any correlation in inhibitor potency between insASV or insSVD and WT EGFR (Fig. 2 *A* and *B*), but clear correlation between L858R and the WT kinase (Fig. 2*C*). Consistent with the drug-sensitizing effect of the L858R mutation, most of the points in this plot fell below the line of equipotency, reflecting the greater potency against L858R EGFR as compared with WT EGFR. Similarly, comparisons between the three exon 20 insertion variants revealed clear correlation in their sensitivity to this panel of inhibitors (Fig. 2 *D*–*F*).

Table 2. Inhibitor potencies across EGFR variants*

		IC_{50} (nM)					
		WT	L858R	L858R/T790M	insASV	insSVD	insNPG
1st Gen	Gefitinib	>1,000	40 ± 12	>1,000	>1,000	>1,000	>1,000
	Lapatinib	0.5 ± 0.2	3.5 ± 1.0	>1,000	136 ± 60	212 ± 122	9.9 ± 5.9
2nd Gen	Afatinib	2.6 ± 1.2	0.7 ± 0.1	3.0 ± 0.6	>1,000	>1,000	267 ± 31
	Neratinib	0.5 ± 0.2	0.3 ± 0.1	14 ± 6	33 ± 13	348 ± 250	11 ± 5
3rd Gen	Osimertinib	9.6 ± 0.2	6.0 ± 3.6	1.3 ± 0.6	2.4 ± 0.5	2.6 ± 0.2	11.8 ± 6.7
	Olmutinib	73 ± 32	25 ± 6	1.2 ± 0.3	69 ± 21	122 ± 43	44 ± 4
	WZ4002	63 ± 26	16 ± 3	2.6 ± 0.7	105 ± 39	126 ± 31	68 ± 7
	Naquotinib	79 ± 54	13 ± 3	1.2 ± 0.3	133 ± 18	409 ± 192	74 ± 18
	Mavelertinib	4.3 ± 1.6	3.8 ± 0.8	3.2 ± 0.9	14 ± 3	24 ± 8	11 ± 2
	Nazartinib	56 ± 22	19 ± 4	6.2 ± 1.6	150 ± 48	304 ± 130	78 ± 11
4th Gen	BI-4020	>1,000	69 ± 18.4	0.4 ± 0.1	>1,000	>1,000	427 ± 32
Allosteric	EAI045	>1,000	9.3 ± 1.7	10 ± 2.6	>1,000	>1,000	>1,000
	EAI002	>1,000	861 ± 188	167 ± 31	>1,000	>1,000	>1,000
	JBJ-09-063	1.5 ± 0.6	0.8 ± 0.2	0.9 ± 0.2	28 ± 6	192 ± 68	20 ± 1
Exon 20	BAY-33	>1,000	4.5 ± 1.0	227 ± 132	2.4 ± 0.5	3.8 ± 1.2	2.1 ± 0.4
	BAY-568	>1,000	28.3 ± 38.4	>1,000	0.09 ± 0.03	0.21 ± 0.04	0.11 ± 0.07
	TAS6417	34 ± 25	3.2 ± 0.6	1.1 ± 0.3	16 ± 4	6.0 ± 1.9	4.1 ± 0.4
	Poziotinib	0.3 ± 0.1	0.7 ± 0.2	0.9 ± 0.2	0.6 ± 0.2	0.9 ± 0.3	0.3 ± 0.1
	TAK-788	4.4 ± 1.5	0.6 ± 0.1	0.6 ± 0.2	1.4 ± 0.4	1.7 ± 0.4	1.3 ± 0.3
	BDTX-189	0.3 ± 0.1	0.3 ± 0.1	1.5 ± 0.3	2.1 ± 0.7	55 ± 18	0.8 ± 0.1

*IC_{50} values provided are mean, ±SD of n = 3 independent experiments, each conducted in triplicate.

Cellular Activity of EGFR Exon 20 Inhibitors against Insertion Variants. We sought to extend our biochemical results by treating Ba/F3 cells expressing WT EGFR, EGFR insASV, and insSVD with EGFR exon 20 inhibitors to assess their cellular potencies and mutant selectivities (Fig. 3). In measurements of cell viability, we observed that BAY-568, TAK-788, and TAS6417 were both potent and selective for insASV and insSVD compared to WT EGFR, and displayed similar selectivity trends as in the biochemical studies (Fig. 3 *A*–*C* and *G*). Poziotinib displayed marginally higher potency against WT EGFR than against insASV or insSVD, while BDTX-189 was similarly potent against WT EGFR and the insertion variants. Although BAY-33 was potent in biochemical assays (~2 nM IC_{50}), it was not potent in these cell-based assays (~2 μM against exon 20 insertions), possibly due to poor cell permeability. BAY-568, a structural analog of BAY-33 with a fluorine replacing a chlorine, exhibited both potent and selective inhibition of insASV or insSVD (>sixfold selective versus WT EGFR).

We also assessed cellular signaling in these Ba/F3 models 6 h after inhibitor treatment at 25 or 100 nM by western blotting with phospho-specific antibodies for EGFR, ERK, and AKT activation (p-EGFR Y1068, p-ERK1/2, and p-Akt S473, Fig. 3 *D*–*F*). These studies revealed inhibition of pEGFR and

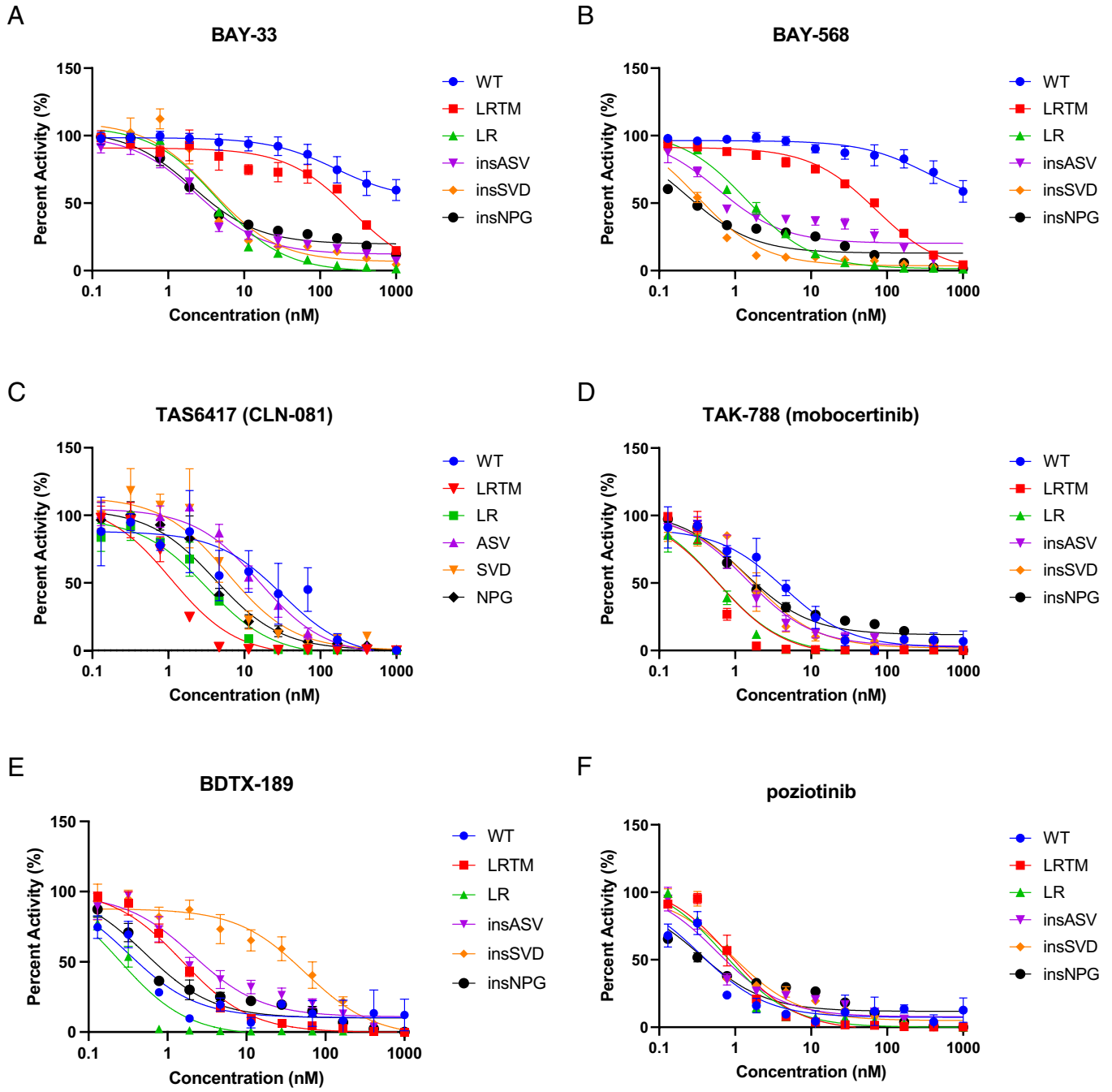

Fig. 1. Biochemical inhibition curves for EGFR exon 20 insertion inhibitors. (*A*–*F*) Concentration–response curves for inhibition of WT EGFR and the L858R, L858R/T790M, insASV, insSVD, and insNPG variants by the indicated inhibitor. Data were normalized to enzyme activity when no inhibitor is present, and data points are shown as mean ± SD, n = 3. The experiment was performed three times, each time in triplicate. A representative triplicate experiment is shown.

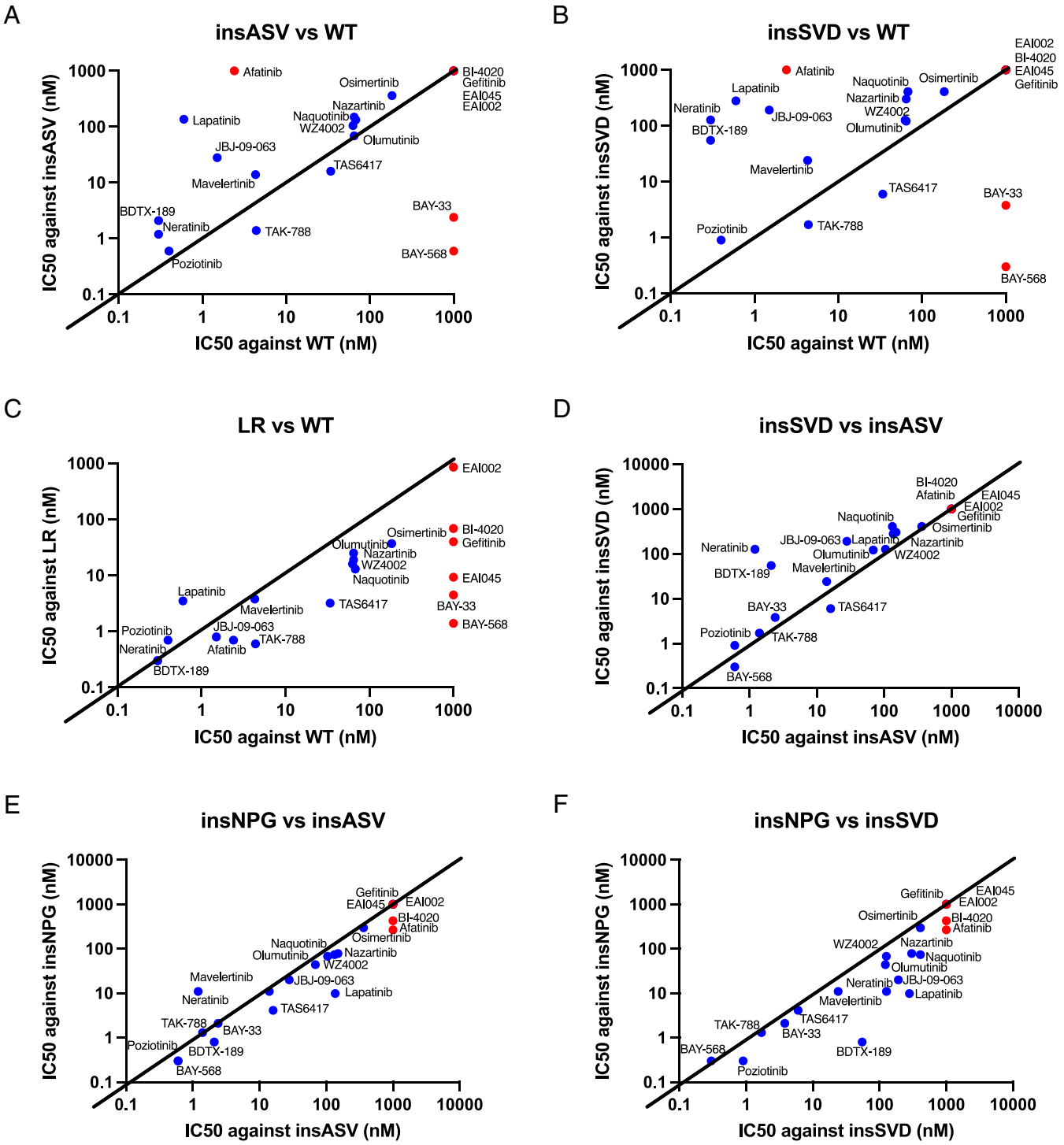

Fig. 2. Comparison of biochemical potency of EGFR inhibitors against different EGFR variants. (*A*–*F*) Correlation plots showing pairwise comparison of inhibitor IC_{50} values across WT and selected EGFR variants, as indicated, for the 20 inhibitors studied here. Each compound is plotted with its *x*-axis value corresponding to its IC_{50} against the first EGFR variant and its *y*-axis value corresponding to its IC_{50} against the second EGFR variant. Red dots indicate compounds with one or both IC_{50} values beyond the range of the assay (>1 μM). The diagonal black line indicates equipotency (x = y) and is shown for easier identification of mutant-selective compounds.

downstream effectors pERK1/2 and pAKT that correlated well with the cell viability studies. For example, BAY-568 at 100 nM substantially inhibited pEGFR, pERK1/2, and pAkt in insASV and insSVD Ba/F3 cells, but inhibition of pEGFR was incomplete in Ba/F3 cells expressing WT EGFR and pERK1/2 and pAkt were only modestly decreased (Fig. 3 *D*–*F*). By contrast, poziotinib and BDTX-189 at 100 nM suppressed signaling indiscriminately across all three cell lines.

Crystal Structures of EGFR Kinase in Complex with Exon 20 Inhibitors. As we have been unable to obtain suitable crystals of the insASV or insSVD variants, we determined cocrystal structures of BAY-33, TAK-788, TAS6417, and poziotinib with WT EGFR to better understand their binding modes and molecular determinants of their potencies. We also determined a cocrystal structure of poziotinib with T790M/V948R EGFR (Fig. 4 and *SI Appendix*, Fig. S5 and Table S1).

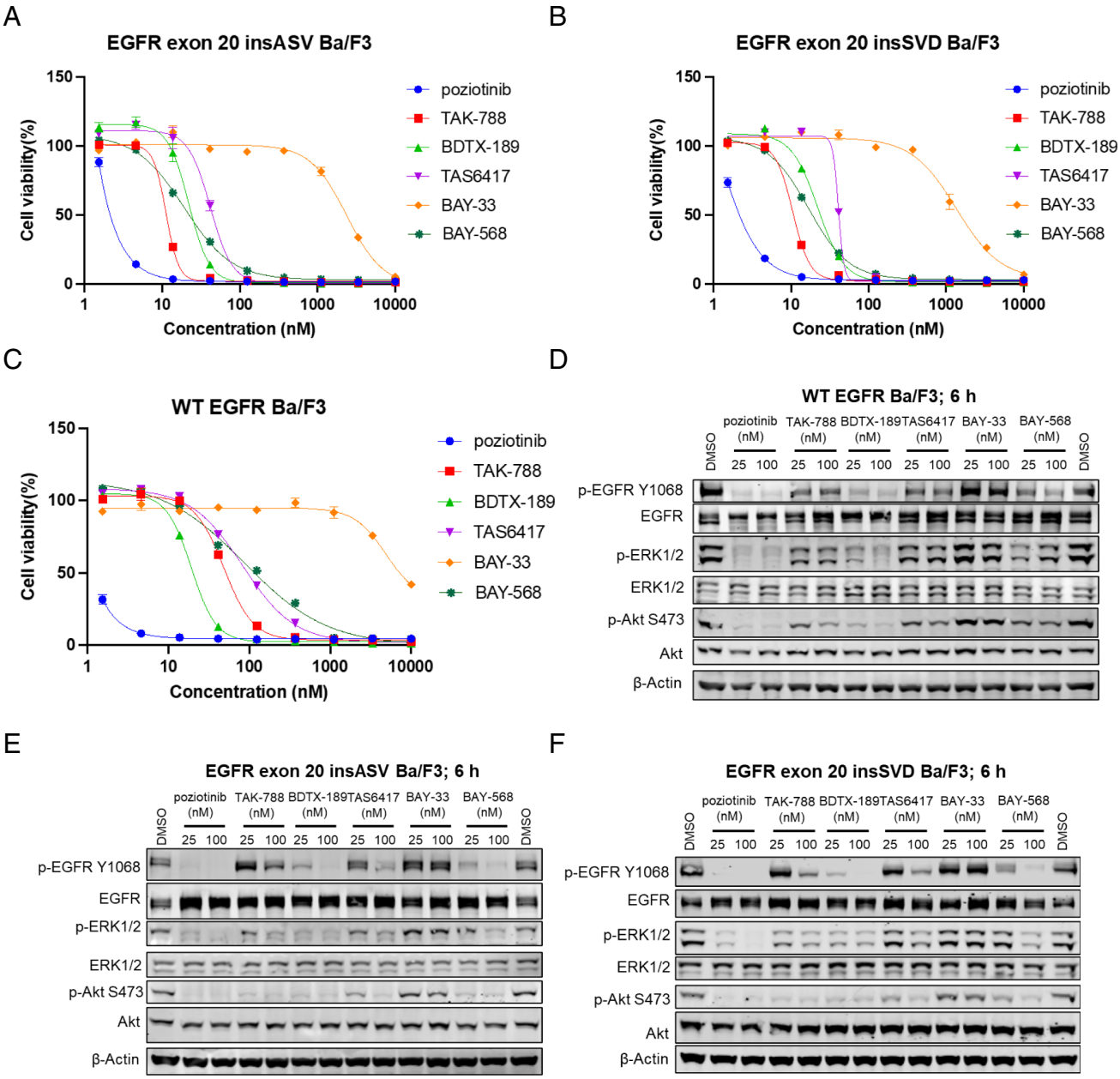

G

	WT EGFR IC50 (nM)	insASV IC50 (nM)	insSVD IC50 (nM)
poziotinib	0.8 ± 0.3	2.7 ± 0.1	2.4± 0.1
TAK-788	53 ± 4	12 ± 1	11 ± 0.7
BDTX-189	21 ± 1	27 ± 5	25 ± 2
TAS6417	101 ± 10	42 ± 3	41 ± 1
BAY-33	7860 ± 1191	2360 ± 240	1598 ± 228
BAY-568	128 ± 20	24 ± 2	20 ± 1

Fig. 3. Cellular potency of exon 20 inhibitors. (*A–C*) Dose-dependent cell growth inhibition of Ba/F3 cells expressing EGFR D770_N771insNPG, D770_N771insSVD, or WT EGFR in the presence of 50 ng/mL EGF. Ba/F3 cells expressing aforementioned EGFR mutations were treated with the indicated doses of exon 20 inhibitors for 72 h. Cell survival was measured using a CellTiter Aqueous One Solution Cell Proliferation Assay. Error bars indicate SD (n = 3). (*D–F*) Western blot analysis of the effects of exon 20 inhibitors on Ba/F3 cells expressing EGFR insNPG, insSVD, or WT EGFR in the presence of 50 ng/mL EGF. The cells were treated with indicated doses of inhibitors for 6 h. Phosphorylation of EGFR, AKT, and ERK proteins was detected by immunoblotting. (*G*) Table showing cellular IC_{50} values for these exon 20 inhibitors against Ba/F3 cells expressing WT, insASV, or insSVD EGFR.

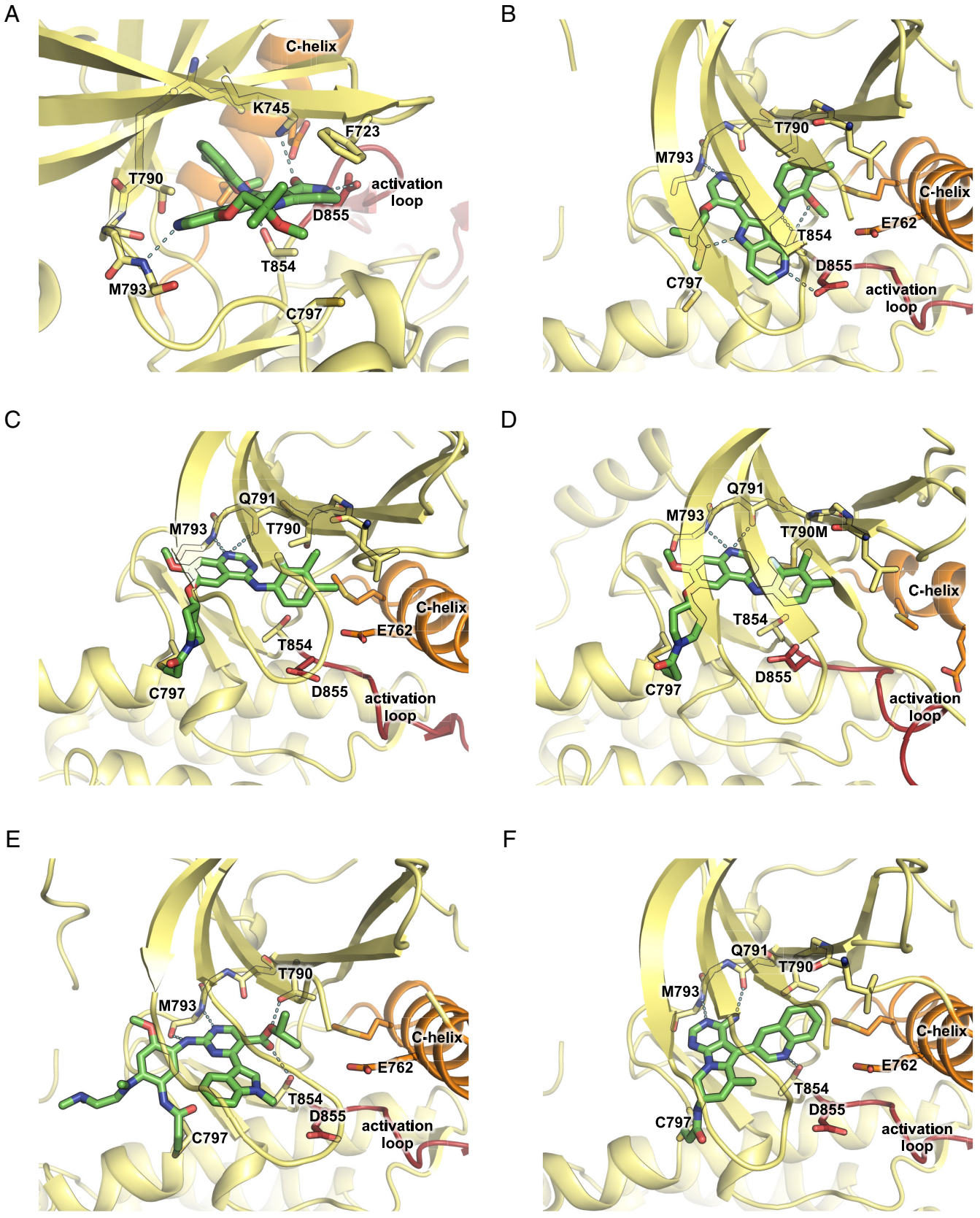

Fig. 4. Crystal structures of EGFR kinase in complex with exon 20 inhibitors. In (*A*–*F*) EGFR is shown in a yellow ribbon representation with the C-helix colored orange and the activation loop red. Dashed lines indicate hydrogen bonds. (*A*) View of active site for WT EGFR in complex with BAY-33 showing interactions with the hinge region, C-helix, and F723 (PDB 8F1Z) (46). (*B*) Alternate view of BAY-33 (PDB 8F1Z). (*C*) Interactions of poziotinib in the active site of WT EGFR (PDB 8F1Y) (47). (*D*) Interactions of poziotinib in the active site of EGFR T790M/V948R (PDB 8F1W) (48). Note that the kinase adopts an inactive conformation in this structure, with the C-helix displaced in an outward position. (*E*) Interactions of TAK-788 in WT EGFR (PDB 8F1X) (49). (*F*) View of the interactions of TAS6417 in the active site of WT EGFR (PDB 8F1H) (50).

BAY-33 binds with its pyridine group adjacent to the hinge region of the kinase, where it forms a single hydrogen bond with the backbone amide of M793 (Fig. 4 *A* and *B*). The fluoro- and methoxy- substituted anilino group packs against the gatekeeper residue T790 (Fig. 4*B*). This interaction is generally similar to that of anilinoquinazoline inhibitors (e.g., gefitinib) in this region, but the trajectory into the pocket is rather different due to the divergent scaffold of BAY-33. The aniline nitrogen hydrogen bonds with the sidechain of T854, and a third hydrogen bond is formed to D855 in the DFG motif. The active site lysine (K745) is positioned to form a fourth hydrogen both with the oxygen in the pyrrolopyridinone scaffold. Interestingly, The side chain of F723 in the phosphate-binding loop (P-loop) folds under the P-loop, and stacks atop the pyrrolopyridinone core of the inhibitor (Fig. 4*A*). Finally, we note the presence of an intramolecular hydrogen bond between the pyrrolo nitrogen and the methoxy oxygen in the "tail" of the inhibitor (Fig. 4*B*). This intramolecular interaction may contribute to affinity by rigidifying the compound in the conformation required for binding.

Poziotinib is an anilinoquinazoline inhibitor and binds in the manner expected for this compound class, with a single hydrogen bond to the hinge region, and the halogen-substituted aniline group in the back pocket adjacent to the gatekeeper residue (Fig. 4 *C* and *D*). As expected, a covalent bond is formed with C797 at the front edge of the inhibitor binding pocket. We observe a similar binding mode in both the WT and T790M/V948R mutant structures, despite the fact that the latter adopts an inactive kinase conformation (the V948R substitution prevents formation of the activating asymmetric dimer interaction in the crystal lattice, allowing crystallization in the inactive state). The binding mode of poziotinib we observe is essentially the same as that in a recently reported structure with T790M/V948R (51).

The core of TAK-788, which is identical to osimertinib, binds in essentially the same manner as osimertinib and the additional isopropyl ester of TAK-788 extends into the back pocket alongside the gatekeeper T790 and simultaneously hydrogen bonds with both T790 and T854 (Fig. 4*E*). The isopropyl group is in hydrophobic contact with V726 and K745. The binding mode of TAK-788 in the present structure is similar to that in recently described structures of this compound in complex with WT and mutant EGFR, but a different rotamer of the isopropyl ester in the prior structures leads to differences in its hydrogen bonding to T790 and T854 (51, 52).

In the TAS6417 structure, the tricyclic core of the inhibitor forms dual hydrogen bonds to the kinase hinge, and the acrylamide forms the expected covalent bond with C797 (Fig. 4*F*). The quinoline substituent extends into the back pocket between T790 and K745, and the quinoline nitrogen hydrogen bonds with T854. The quinoline group fills much the same space as the isopropyl ester in TAK-788, but it extends deeper into the pocket and is in hydrophobic contact with L799 in addition to T790 and K745.

Discussion

Lung cancers driven by EGFR exon 20 insertion mutations represent an ongoing therapeutic challenge. Clinical development of poziotinib, BDTX-189, and TAK-788 has been discontinued. Bayer compound BAY2927088 is being evaluated in EGFR- and Her2-altered NSCLC (38) and has received FDA Breakthrough Therapy designation, but only for certain patients with activating Her2 mutations (53). Therefore, development of potent, exon 20 insertion-selective EGFR inhibitors remains a priority. Mutant-selectivity versus WT EGFR is a requirement for an effective and tolerable therapeutic in this indication, and in this study, we have undertaken a side-by-side comparison of the potency and mutant-selectivity of a diverse panel EGFR TKIs against insASV, insSVD, and WT EGFR using a biochemical approach.

Among the compounds we tested, we find that BAY-568 was most potent and selective against insASV and insSVD, although the fold-selectivity observed in Ba/F3 cell assays was not as pronounced as in biochemical kinase inhibition assays. It is unclear whether this compound is being considered for clinical development. TAK-788 and TAS6417 were also potent and selective versus WT EGFR, but with a narrower margin as compared with BAY-33 and BAY-568. By contrast, poziotinib and BDTX-189 were as potent against WT EGFR as they were against any of the mutants studied here.

Structural analysis of diverse exon 20 insertion inhibitors with WT EGFR reveals common features that contribute to their potency. We note that the mutant-selective inhibitors BAY-33, TAS6417, and TAK-788 all place a hydrophobic group adjacent to the gatekeeper residue T790 and all hydrogen bond with T854. Thus, these features are likely to be important contributors to potency against the insertion mutants. In further support of this notion, the Rauh group has recently described LDC0496, a potent exon 20 insertion inhibitor that positions an isopropyl ester similarly to TAK-788, but from an entirely different scaffold (51). The structural basis for the selectivity of these agents, however, remains unclear. While we lack crystal structures of insASV and insSVD, our previous structure of insNPG reveals essentially no changes in the inhibitor binding site as compared to WT (28). Comparison of recent crystal structures of TAK-788 with WT and insNPG EGFR revealed only a small change in the orientation of C755 in the mutant (52). While this residue is adjacent to the isopropyl ester of TAK-788 and could in principle contribute to selectivity, it is unclear whether or how the insertion may affect its orientation. Molecular dynamics studies reveal altered dynamics of N- and C-lobe orientations in the exon20 insertion variants, and such differences could underlie altered inhibitor sensitivity (54).

Very recently, Astrazeneca reported development of AZ14133346, a compound with 14-fold selectivity for EGFR insSVD versus WT EGFR (55). Interestingly, crystal structures with a close analog of this compound in WT and insNPG EGFR show that it binds or induces an unusual conformation of the kinase that resembles the inactive, C-helix-out state. While the WT and insNPG structures in complex with this compound are globally similar, there are distinct interactions with the compound in the insertion mutant (in particular with Met766 in the displaced C-helix) that appear to contribute to its mutant-selectivity (55).

Our biochemical findings highlight an important distinction between the L858R EGFR and the insASV and insSVD exon20 insertion variants: Inhibitor sensitivity of the L858R point mutant is closely correlated with that of WT EGFR, while that of the insertion variants is not. In effect, they behave more like different kinases. This suggests that screening for novel inhibitor scaffolds potent against the insertion variants but with little activity against WT EGFR may be a more productive route to discovery of new agents than refinement of established EGFR inhibitor scaffolds. In this regard, it is interesting to note that BDTX-189 and poziotinib are essentially 2nd generation EGFR TKIs and TAK-788 builds on 3rd generation inhibitor osimertinib, while BAY-568 and AZ14133346 have been developed as novel agents for exon 20 variants (37). Finally, we find that inhibitor potency against the three insertion variants examined here is highly correlated, suggesting that a drug developed for this indication is likely to be effective against many of these diverse alterations.

Materials and Methods

Inhibitors. EAI002, EAI045, and JBJ-09-063 were synthesized in-house for prior studies (23, 24, 56). BAY-33 corresponds to example #33 in patent WO2019081486 and was synthesized by PepTech Corp. (>95% pure). All other inhibitors used in this study were purchased from commercial vendors and are >95% pure per the vendors' analyses. Compound stocks were prepared in DMSO and stored at −20 °C.

Cloning, Expression, and Purification of EGFR Kinase Domain. EGFR V769_D770insASV and D770_N771insSVD with residues ranging from 696 to 1,022 (WT numbering) were expressed and purified in Sf9 insect cells using the Baculogold system (Pharmingen). EGFR L858R, L858R/T790M, T790M/V948R, D770_N771insNPG, and WT with construct residues 696 to 1,022 were expressed and purified in a similar way, as described previously (28, 57, 58). EGFR mutant constructs were first introduced into the human *EGFR* wild-type (WT) sequence in the context of the pAC8 vector using the QuickChange XL site-Directed Mutagenesis Kit (Stratagene) or gene blocks ordered from IDT DNA. The resulting constructs were confirmed by Sanger sequencing and were expressed as N-10× His C-TwinStrep fusion proteins.

Cell pellets of insASV or insSVD were lysed by sonication in 50 mM Tris-HCl (pH 8.0), 500 mM NaCl, and 20% glycerol supplemented with 1 mM TCEP [tris(2-carboxyethyl) phosphine hydrochloride], 20 mM imidazole, and complete protease inhibitor mixture (Roche). After centrifugation (40,000 rpm, 2 h, 4 °C), the supernatant was loaded to an Ni-NTA column and flown through. The beads were washed with wash buffer (50 mM Tris-HCl, 500 mM NaCl, 20% Glycerol, 50 mM imidazole, 1 mM TCEP [pH 8.0]) and then eluted with elution buffer (50 mM Tris-HCl, 500 mM NaCl, 20% Glycerol, 200 mM imidazole, 1 mM TCEP [pH 8.0]). The eluted EGFR kinases (not concentrated) were further purified by size-exclusion chromatography (Superdex 200) in SEC buffer (50 mM Tris-HCl, 500 mM NaCl, 20% Glycerol, 1 mM TCEP [pH 8.0]) and were concentrated to 30 μg/mL (insASV) or 80 μg/mL (insSVD), and aliquots were flash frozen in liquid nitrogen and stored at −80 °C. EGFR WT, L858R, L858R/T790M, T790M/V948R, and insNPG were purified as described previously (17, 28).

Crystallization and Structure Determination. Purified EGFR kinase domain with affinity tags cleaved was crystallized via the hanging drop method at room temperature. EGFR(T790M/V948R) at ~3 mg/mL was supplemented with 1 mM adenylyl-imidodiphosphate (AMP-PNP) and 10 mM $MgCl_2$ and drops containing 1 μL protein+1 μL well solution were set above wells containing 0.1 M Bis-Tris pH = 5.7 and 25 to 30% (w/v) PEG 3,350. WT EGFR was similarly crystallized in the presence of 1 mM AMP-PNP and 10 mM $MgCl_2$ over wells containing 0.1 M MES pH 6.5 and 0.9 to 1.2 M sodium citrate. Inhibitors were soaked into crystals overnight at a concentration of 1 mM except for BAY-33 for which solid compound was added to the drop containing crystals. Crystals were cryoprotected in well solution supplemented with 20% ethylene glycol prior to flash freezing in liquid nitrogen.

Diffraction data were collected at the Advanced Photon Source at the Argonne National Laboratory on NE-CAT beamlines 24-ID-C and 24-ID-E at 100 K. Data were indexed, integrated, and scaled using Dials and xia2 compiled by SBGrid (59–61). Structures were phased via molecular replacement and refined using Phenix with iterative rounds of manual model building in Coot (62, 63). Ligand restraints were generated using eLBOW in Phenix using the AM1 quantum mechanical optimization method (64). Structures have been deposited in the Protein Data Bank (PDB) with the accession codes 8F1H, 8F1W, 8F1X, 8F1Y, and 8F1Z (46–50).

EGFR Enzyme Kinetic Assays. For in vitro enzyme kinetic and inhibition studies, WT or mutant EGFR kinases (residues 696 to 1,022 of the human EGFR) were expressed and purified in Sf9 insect cells. Kinetic parameters were determined using the ATP/NADH coupled assay system in a 96-well plate, as described previously (13). Briefly, the reaction mixture contained 0.5 mg/mL BSA, 2 mM $MnCl_2$, 1 mM phosphoenolpyruvate (PEP), 1 mM TCEP, 1 mM ATP, 0.1 M HEPES 7.5, 1/50 volume of PK/LDH, 0.5 mM NADH, 1 mM tyrosine kinase substrate poly-[Glu4Tyr], in addition to the indicated EGFR mutant. WT or mutant EGFR kinases were used at the following concentrations: 30 nM (L858R), 60 nM (L858R/T790M), 500 nM (D770_N771insSVD), 100 nM (V769_D770insASV), and 1 μM (WT). ATP at the indicated concentration was added last to start the reaction. Steady-state initial velocity data were drawn from the slopes of the A340 curves and fit to the Michaelis–Menten equation in GraphPad Prism to determine kcat and Km values. The active enzyme concentrations of each mutant were determined by titration with the irreversible inhibitor poziotinib (13, 30).

EGFR Inhibition Assay. Inhibition assays were performed using the HTRF KinEASE tyrosine kinase assay kit (Cisbio) according to the manufacturer's protocol. Inhibitors (10 mM DMSO stocks) were dispensed into black 384-well plates using an HP D300e dispenser (Hewlett-Packard) and normalized to a 1% final DMSO concentration. For inhibitor experiments, assay buffer containing purified EGFR at a final concentration of 5 nM (WT EGFR) or 0.5 nM (L858R, L858R/T790M, D770_N771insSVD, and V769_D770insASV) was dispensed using a Multidrop Combi dispenser (ThermoFisher) and incubated with compounds at room temperature for 30 min. Reactions were initiated with 1 mM ATP and allowed to proceed for 30 min (WT) or 10 min (mutants) at room temperature before being quenched using the detection reagent from the HTRF KinEASE assay kit. The FRET signal ratio was measured at 665 and 620 nm using a PHERAstar microplate reader (BMG LABTECH). Data were processed using GraphPad Prism and fit to a three-parameter dose–response model with the Hill slope constrained to −1.

Ba/F3 Cell Culture and Antiproliferation Assay. EGFR exon 20 insASV Ba/F3 and EGFR exon 20 insSVD Ba/F3 cells were cultured in RPMI media (Life technologies, Cat# 11875119) containing 10% fetal bovine serum (Life technologies, Cat#10437028) and 1% Penicillin/Streptomycin (Life technologies, Cat#10378016). WT EGFR Ba/F3 cells were cultured in RPMI media containing 10 ng/mL EGF (Life Technologies, cat # PHG0311L),10% fetal bovine serum, and 1% Penicillin/Streptomycin. All the cell lines were cultured at 37 °C in 5% CO2 humidified air and tested for *Mycoplasma* negative.

EGFR exon 20 insASV Ba/F3, EGFR exon 20 insSVD Ba/F3, and WT EGFR Ba/F3 (+50 ng/mL EGF) cells were seeded at the density of 1,000 cells/well in 384-well plates. The compounds were added to the cells and incubated for 72 h. Cell viability was determined by using CellTiter-Glo (Promega #G7571) according to the manufacturer's instructions, measuring luminescence using an Envision plate-reader (PerkinElmer Inc.). Dose–response curves were generated using nonlinear regression curve fit in GraphPad Prism 9 (GraphPad Software).

Immunoblotting and Antibodies. Cells were lysed in RIPA buffer (150 mM NaCl, 1.0% IGEPAL® CA-630, 0.5% sodium deoxycholate, 0.1% SDS, 50 mM Tris, pH 8.0) (Sigma, Cat# R0278) with protease inhibitor and phosphatase inhibitor (Roche). The protein concentrations were measured by BCA analysis (Thermo Fisher Scientific, Cat # PI23225). Equal amounts of protein were resolved by 4 to 12% Tris-Base gels (Life Technologies), and then transferred to the Immuno-Blot PVDF membrane (BioRad, cat # 1620177). Proteins were probed with appropriate primary antibodies at 4 °C overnight and then with IRDye®800-labeled goat anti-rabbit IgG (LICOR Biosciences, cat # 926-32211), IRDye®800-labeled goat anti-mouse IgG (LICOR Biosciences, cat # 926-32210) or IRDye 680RD goat anti-Mouse IgG (LICOR Biosciences, Cat # 926-68070) secondary antibodies at room temperature for 1 h. The membranes were detected on Odyssey CLx system.

Antibodies against the following proteins were used in this study: EGFR (Cell signaling Technology, #4267S, 1:1,000), p-EGFR (Tyr1068) (Cell signaling Technology, #3777S, 1:1,000), ERK1/2 (Cell signaling Technology, #4696S, 1:0000), p-ERK1/2 (Cell Signaling Technology, #4370S, 1:1,000), Akt (Cell signaling Technology, #9272L, 1:1,000), p-Akt (Cell Signaling Technology, #4060S, 1:1,000), and β-Actin (Cell Signaling Technology, #3700, 1:1,000).

Data, Materials, and Software Availability. Crystal structure data have been deposited in the Protein Data Bank and are available at www.rcsb.org with accession codes: 8F1H (50), 8F1W (48), 8F1X (49), 8F1Y (47), and 8F1Z (46).

ACKNOWLEDGMENTS. Portions of this paper were developed from the doctoral dissertation of H.Z. (https://nrs.harvard.edu/URN-3:HUL.INSTREPOS:37375468). We thank Milka Kostic for her critical evaluation of this manuscript. We also thank Dongman Jang for his assistance with making structural figures. This work was supported by the NIH grant R01 CA201049 (M.J.E.), P01 CA154303 (P.A.J. and M.J.E.), R35 CA242461 (M.J.E.), and R35 CA220497 (P.A.J.). H.Z. was supported by Chleck Fellowship. T.S.B. was supported by a Ruth L. Kirschstein National Research Service Award (F32CA247198). This work is based upon research conducted at the Northeastern Collaborative Access Team beamlines (P30 GM124165, P41 GM103403) utilizing resources of the Advanced Photon Source at the Argonne

National Laboratory (DE-AC02-06CH11357). The Eiger16M detector on 24-ID-E is funded by an NIH-ORIP HEI grant (S10OD021527).

Author affiliations: [a]Department of Cancer Biology, Dana-Farber Cancer Institute, Boston, MA 02215; [b]Department of Biological Chemistry and Molecular Pharmacology, Harvard Medical School, Boston, MA 02115; [c]Lowe Center for Thoracic Oncology, Dana-Farber Cancer Institute, Boston, MA 02215; [d]Department of Medical Oncology, Dana-Farber Cancer Institute, Boston, MA 02215; and [e]Department of Medicine, Harvard Medical School, Boston, MA 02115

Author contributions: H.Z., T.S.B., J.J., P.A.J., and M.J.E. designed research; H.Z., T.S.B., J.J., J.K.R., I.K.S., and J.S. performed research; H.Z., T.S.B., J.J., P.A.J., and M.J.E. analyzed data; and H.Z., T.S.B., J.J., P.A.J., and M.J.E. wrote the paper.

Competing interest statement: M.J.E. receives or has received sponsored research support from Novartis, Sanofi, Takeda, and Springworks Therapeutics and consulting income or honoraria from Novartis, H3 Biomedicine and Ikena Oncology. P.A.J. has received consulting fees from AstraZeneca, Boehringer Ingelheim, Pfizer, Roche/Genentech, Takeda Oncology, ACEA Biosciences, Eli Lilly and Company, Araxes Pharma, Ignyta, Mirati Therapeutics, Novartis, LOXO Oncology, Daiichi Sankyo, Sanofi Oncology, Voronoi, SFJ Pharmaceuticals, Biocartis, Novartis Oncology, Nuvalent, Esai, Bayer, Transcenta, Silicon Therapeutics, Allorion Therapeutics, Accutar Biotech and AbbVie; receives post-marketing royalties from DFCI-owned intellectual property on EGFR mutations licensed to Lab Corp; receives or has received sponsored research funding from AstraZeneca, Astellas, Daichi-Sankyo, PUMA, Boehringer Ingelheim, Eli Lilly and Company, Revolution Medicines and Takeda and has stock ownership in Gatekeeper Pharmaceuticals. H.Z. was a consultant at Boston Consulting Group and is currently a consultant at Bain & Company. All other authors declare no competing interests.

1. H. Sung *et al.*, Global cancer statistics 2020: GLOBOCAN estimates of incidence and mortality worldwide for 36 cancers in 185 countries. *CA Cancer J. Clin.* **71**, 209–249 (2021).
2. R. L. Siegel, K. D. Miller, H. E. Fuchs, A. Jemal, Cancer statistics. *CA Cancer J. Clin.* **71**, 7–33 (2021).
3. T. J. Lynch *et al.*, Activating mutations in the epidermal growth factor receptor underlying responsiveness of non–small-cell lung cancer to gefitinib. *N. Engl. J. Med.* **350**, 2129–2139 (2004).
4. J. G. Paez *et al.*, EGFR mutations in lung, cancer: Correlation with clinical response to gefitinib therapy. *Science* **304**, 1497–1500 (2004).
5. R. Sordella, D. W. Bell, D. A. Haber, J. Settleman, Gefitinib-sensitizing EGFR mutations in lung cancer activate anti-apoptotic pathways. *Science* **305**, 1163–1167 (2004).
6. B. Melosky *et al.*, Worldwide prevalence of epidermal growth factor receptor mutations in non-small cell lung cancer: A meta-analysis. *Mol. Diagn. Ther.* **26**, 7–18 (2022).
7. H. Yasuda, S. Kobayashi, D. B. Costa, EGFR exon 20 insertion mutations in non-small-cell lung cancer: Preclinical data and clinical implications. *Lancet Oncol.* **13**, e23–e31 (2012).
8. G. R. Oxnard *et al.*, Natural history and molecular characteristics of lung cancers harboring EGFR exon 20 insertions. *J. Thorac. Oncol.* **8**, 179 (2013).
9. M. E. Arcila *et al.*, EGFR exon 20 insertion mutations in lung adenocarcinomas: Prevalence, molecular heterogeneity, and clinicopathologic characteristics. *Mol. Cancer Ther.* **12**, 220 (2013).
10. W. Pao *et al.*, EGF receptor gene mutations are common in lung cancers from "never smokers" and are associated with sensitivity of tumors to gefitinib and erlotinib. *Proc. Natl. Acad. Sci. U.S.A.* **101**, 13306 (2004).
11. L. V. Sequist, D. W. Bell, T. J. Lynch, D. A. Haber, Molecular predictors of response to epidermal growth factor receptor antagonists in non-small-cell lung cancer. *J. Clin. Oncol.* **25**, 587–595 (2007).
12. R. T. Dungo, G. M. Keating, Afatinib: First global approval. *Drugs* **73**, 1503–1515 (2013).
13. C. H. Yun *et al.*, Structures of lung cancer-derived EGFR mutants and inhibitor complexes: Mechanism of activation and insights into differential inhibitor sensitivity. *Cancer Cell* **11**, 217–227 (2007).
14. K. D. Carey *et al.*, Kinetic analysis of epidermal growth factor receptor somatic mutant proteins shows increased sensitivity to the epidermal growth factor receptor tyrosine kinase inhibitor, erlotinib. *Cancer Res.* **66**, 8163–8171 (2006).
15. I. K. van Alderwerelt *et al.*, Biochemical and structural basis for differential inhibitor sensitivity of EGFR with distinct exon 19 mutations. *Nat. Commun.* **13**, 6791 (2022).
16. M. J. Eck, C. H. Yun, Structural and mechanistic underpinnings of the differential drug sensitivity of EGFR mutations in non-small cell lung cancer. *Biochim. Biophys. Acta* **1804**, 559–566 (2010).
17. C. H. Yun *et al.*, The T790M mutation in EGFR kinase causes drug resistance by increasing the affinity for ATP. *Proc. Natl. Acad. Sci. U.S.A.* **105**, 2070–2075 (2008).
18. W. Zhou *et al.*, Novel mutant-selective EGFR kinase inhibitors against EGFR T790M. *Nature* **462**, 1070–1074 (2009).
19. D. A. E. Cross *et al.*, AZD9291, an irreversible EGFR TKI, overcomes T790M-mediated resistance to EGFR inhibitors in lung cancer. *Cancer Discov.* **4**, 1046–1061 (2014).
20. S. L. Greig, Osimertinib: First global approval. *Drugs* **76**, 263–273 (2016).
21. S. S. Ramalingam *et al.*, Osimertinib as first-line treatment of EGFR mutation-positive advanced non-small-cell lung cancer. *J. Clin. Oncol.* **36**, 841–849 (2018).
22. J.-C. Soria *et al.*, Osimertinib in untreated EGFR-mutated advanced non-small-cell lung cancer. *N. Engl. J. Med.* **378**, 113–125 (2018).
23. Y. Jia *et al.*, Overcoming EGFR T790M and C797S resistance with mutant-selective allosteric inhibitors. *Nature* **534**, 129 (2016).
24. C. To *et al.*, An allosteric inhibitor against the therapy-resistant mutant forms of EGFR in non-small cell lung cancer. *Nat. Cancer* **3**, 402–417 (2022).
25. M. S. Eno *et al.*, Discovery of BLU-945, a reversible, potent, and wild-type-sparing next-generation EGFR mutant inhibitor for treatment-resistant non-small-cell lung cancer. *J. Med. Chem.* **65**, 9662 (2022).
26. K. S. Thress *et al.*, Acquired EGFR C797S mediates resistance to AZD9291 in advanced non-small cell lung cancer harboring EGFR T790M. *Nat. Med.* **21**, 560 (2015).
27. D. Ercan *et al.*, EGFR mutations and resistance to irreversible pyrimidine-based EGFR inhibitors. *Clin. Cancer Res.* **21**, 3913–3923 (2015).
28. H. Yasuda *et al.*, Structural, biochemical and clinical characterization of epidermal growth factor receptor (EGFR) exon 20 insertion mutations in lung cancer. *Sci. Transl. Med.* **5**, 216ra177 (2013).
29. G. J. Riely *et al.*, Activity and safety of mobocertinib (TAK-788) in previously treated non-small cell lung cancer with EGFR exon 20 insertion mutations from a phase I/II trial. *Cancer Discov.* **11**, 1688–1699 (2021).
30. J. P. Robichaux *et al.*, Mechanisms and clinical activity of an EGFR and HER2 exon 20–selective kinase inhibitor in non–small cell lung cancer. *Nat. Med.* **24**, 638–646 (2018).
31. S. Hasako *et al.*, TAS6417, a novel EGFR inhibitor targeting exon 20 insertion mutations. *Mol. Cancer Ther.* **17**, 1648–1658 (2018).
32. S. Vyse, P. H. Huang, Targeting EGFR exon 20 insertion mutations in non-small cell lung cancer. *Signal Transduction Targeted Ther.* **4**, 1–10 (2019).
33. J. Naidoo *et al.*, Epidermal growth factor receptor exon 20 insertions in advanced lung adenocarcinomas: Clinical outcomes and response to erlotinib. *Cancer* **121**, 3212–3220 (2015).
34. M. Yang *et al.*, NSCLC harboring EGFR exon-20 insertions after the regulatory C-helix of kinase domain responds poorly to known EGFR inhibitors. *Int. J. Cancer* **139**, 171–176 (2016).
35. J. C. H. Yang *et al.*, Clinical activity of afatinib in patients with advanced non-small-cell lung cancer harbouring uncommon EGFR mutations: A combined post-hoc analysis of LUX-Lung 2, LUX-Lung 3, and LUX-Lung 6. *Lancet Oncol.* **16**, 830–838 (2015).
36. A. M. Schram *et al.*, Safety and preliminary efficacy from the phase 1 portion of MasterKey-01: A First-in-human dose-escalation study to determine the recommended phase 2 dose (RP2D), pharmacokinetics (PK) and preliminary antitumor activity of BDTX-189, an inhibitor of allosteric ErbB mutations, in patients (pts) with advanced solid malignancies. *J. Clin. Oncol.* **39**, 3086–3086 (2021).
37. F. Siegel *et al.*, Abstract 1470: Preclinical activity of the first reversible, potent and selective inhibitor of EGFR exon 20 insertions. *Cancer Res.* **81**, 1470–1470 (2021).
38. F. Siegel *et al.*, BAY 2927088: The first non-covalent, potent, and selective tyrosine kinase inhibitor targeting EGFR exon 20 insertions and C797S resistance mutations in NSCLC. *Eur. J. Cancer* **174**, S9–S10 (2022).
39. M. Wang *et al.*, Sunvozertinib, a selective EGFR inhibitor for previously treated non-small cell lung cancer with EGFR exon 20 insertion mutations. *Cancer Discov.* **12**, 1676–1689 (2022).
40. J. C.-H. Yang *et al.*, A multinational pivotal study of sunvozertinib in platinum pretreated non-small cell lung cancer with EGFR exon 20 insertion mutations: Primary analysis of WU-KONG1 study. *J. Clin. Oncol.* **42**, 8513–8513 (2024).
41. A. Markham, Mobocertinib: First approval. *Drugs* **81**, 2069–2074 (2021).
42. M. J. Hanley, D. R. Camidge, R. J. Fram, N. Gupta, Mobocertinib: Mechanism of action, clinical, and translational science. *Clin. Transl. Sci.* **17**, e13766 (2024).
43. J. P. Robichaux *et al.*, Structure-based classification predicts drug response in EGFR-mutant NSCLC. *Nature* **597**, 732–737 (2021).
44. A. Kornberg, W. E. Pricer, Enzymatic phosphorylation of adenosine and 2,6-diaminopurine riboside. *J. Biol. Chem.* **193**, 481–495 (1951).
45. S. Siegel *et al.*, "4H-pyrrolo[3,2-c]pyridin-4-one derivatives." WIPO Patent No. 2019081486 (2019).
46. T. S. Beyett, M. J. Eck, Data from "EGFR kinase in complex with Bayer #33." Protein Data Bank. https://www.rcsb.org/structure/8F1Z. Deposited 6 November 2022.
47. T. S. Beyett, M. J. Eck, Data from "EGFR kinase in complex with poziotinib." Protein Data Bank. https://www.rcsb.org/structure/8F1Y. Deposited 6 November 2022.
48. T. S. Beyett, M. J. Eck, Data from "EGFR(T790M/V948R) kinase in complex with poziotinib." Protein Data Bank. https://www.rcsb.org/structure/8F1W. Deposited 6 November 2022.
49. T. S. Beyett, M. J. Eck, Data from "EGFR kinase in complex with mobocertinib (TAK-788)." Protein Data Bank. https://www.rcsb.org/structure/8F1X. Deposited 6 November 2022.
50. T. S. Beyett, M. J. Eck, Data from "EGFR kinase in complex with TAS6417 (CLN-081)." Protein Data Bank. https://www.rcsb.org/structure/8F1H. Deposited 5 November 2022.
51. J. Lategahn *et al.*, Insight into targeting exon20 insertion mutations of the epidermal growth factor receptor with wild type-sparing inhibitors. *J. Med. Chem.* **65**, 6643–6655 (2021), 10.1021/acs.jmedchem.1c02080.
52. W. S. Huang *et al.*, Discovery of mobocertinib, a potent, oral inhibitor of EGFR exon 20 insertion mutations in non-small cell lung cancer. *Bioorg. Med. Chem. Lett.* **80**, 129084 (2023).
53. N. Girard *et al.*, Safety and anti-tumor activity of BAY 2927088 in patients with HER2-mutant NSCLC: Results from an expansion cohort of the SOHO-01 phase I/II study. *J. Clin. Oncol.* **42**, LBA8598 (2024).
54. I. Galdadas *et al.*, Structural basis of the effect of activating mutations on the EGF receptor. *Elife* **10**, e65824 (2021).
55. C. Thomson *et al.*, Discovery and optimization of potent, efficacious and selective inhibitors targeting EGFR exon20 insertion mutations. *J. Med. Chem.* **67**, 8988–9027 (2024).
56. D. J. H. de Clercq *et al.*, Discovery and optimization of Dibenzodiazepinones as allosteric mutant-selective EGFR inhibitors. *ACS Med. Chem. Lett.* **10**, 1549–1553 (2019).
57. D. B. Costa *et al.*, BIM mediates EGFR tyrosine kinase inhibitor-induced apoptosis in lung cancers with oncogenic EGFR mutations. *PLoS Med.* **4**, 1669–1680 (2007).
58. S. Kobayashi *et al.*, EGFR mutation and resistance of non-small-cell lung cancer to gefitinib. *N. Engl. J. Med.* **352**, 786–792 (2005).
59. A. Morin *et al.*, Collaboration gets the most out of software. *Elife* **2**, e01456 (2013).
60. G. Winter *et al.*, DIALS: Implementation and evaluation of a new integration package. *Acta Crystallogr. D Struct. Biol.* **74**, 85–97 (2018).
61. G. Winter, Xia2: An expert system for macromolecular crystallography data reduction. *J. Appl. Crystallogr.* **43**, 186–190 (2010).
62. P. D. Adams *et al.*, PHENIX: A comprehensive Python-based system for macromolecular structure solution. *Acta Crystallogr. D Biol. Crystallogr.* **66**, 213–221 (2010).
63. P. Emsley, B. Lohkamp, W. G. Scott, K. Cowtan, Features and development of Coot. *Acta Crystallogr. D Biol. Crystallogr.* **66**, 486–501 (2010).
64. N. W. Moriarty, R. W. Grosse-Kunstleve, P. D. Adams, electronic Ligand Builder and Optimization Workbench (eLBOW): A tool for ligand coordinate and restraint generation. *Acta Crystallogr. D Biol. Crystallogr.* **65**, 1074 (2009).